31st Congress of the International Council of the Aeronautical Sciences

Belo Horizonte, Brazil; September 09-14, 2018

ON THE EXISTENCE OF MULTIPLE SELF-EXCITATION FREQUENCIES IN THE INSTABILITY OF INTERACTING PLANAR MIXING LAYER AND WAKE

Helio Ricardo de A. Quintanilha Junior* , **Leonardo Santos de Brito Alves****
***University of Liverpool** , ****Universidade Federal Fluminense**

Keywords: *Local Linear Stability Analysis, Self-Excited Frequencies, Convective/Absolute instability, Mixing Layers, Wake*

Abstract

In a recent experiment study about planar mixing layers generated from a thick splitter place, two self-excited frequencies were found in the frequency spectra. However, theoretical and numerical studies of this problem revealed an absolutely unstable region just downstream of the splitter plate containing only a single pinching point associated with the asymmetric mode. The symmetric mode is always found absolutely stable. A local and inviscid linear stability analysis is performed to further investigate this problem. Two separate base flows are constructed to fit the experimental data, extracted from the original experiment study using an image processing code. All nine cases reported in the experiment, with three different velocity ratios and Reynolds number, were reproduced. The analysis reveals two pinching points, one for the symmetric and another for the asymmetric mode, for some cases. In general, there is a good agreement with the experimental frequencies for all nine cases. It appears that the additional pinching strongly depends on the momentum thickness of both layers being different. In all previous theoretical and numerical studies, however, these thicknesses were assumed equal.

1 General Introduction

Hydrodynamic instabilities are present in many problems related to fluid mechanics. In aerospace engineering, the relevant applications are associated with air breathing propulsion engines such as turbojets, ramjets and scramjets, working in subsonic or supersonic state. In order to obtain aerospace propulsion, internal energy can be convert in kinetic energy inside a combustion chamber, generating the necessary impulse. The chemical reactions responsible for generating this internal energy are strongly dependent on the mixing process [1]. Coaxial jet injection systems used in liquid rocket engines, also known as LREs, are one of the most common and largely utilized injectors. In this injector, an inner tube usually carrying liquid oxygen as oxidizer is surrounded by a higher speed stream of either liquid or gaseous hydrogen, usually employed as propellent, which flows through a concentric outer tube. Both fluids are separated by the inner jet tube wall before they come into contact with each other, mix, and combust. This type of injector relies on the shear between these two jets to achieve good mixing.

When two fluids are brought together at the end of the inner jet tube in an incompressible flow, the characteristics of the resulting mixing layer depends strongly several parameters, such as the inner and outer jet velocities, boundary layer thicknesses of the inner and outer flows still inside their respective tubes and the inner tube wall thickness. If the latter is negligible, a classical mixing layer is formed. On the other hand, this wall thickness is not negligible in many practical applications, creating a wake that interacts with the mixing layer. This interaction has

been widely studied in the literature [2-11]. Koch [3] used hyperbolic tangent profiles to study this problem. For symmetric blunt body wakes, a pinching point separating convective and absolute instability was found. Furthermore, an absolute instability region was found just behind the cylinder whereas downstream only convective instability was found. For asymmetric wakes, there was a limit to the asymmetry levels beyond which no absolute instability appears possible. This provides a link to their mixing layers counterparts, where only convective instability occurs. Direct numerical simulation was also performed by Hammoond and Redekopp [5], together as a local instability analysis in a two-dimensional mixing layer wake interaction behind a rectangular body with different vorticity streams. Distributed suction or blowing was imposed at the tip of the body with different velocity streams. However, the momentum thickness employed in the simulation was chosen to be constant to reduce computational cost. Overall, the effect of suction was to reduce the potential for an absolute instability region such that global instability criteria are no longer satisfied and the wake becomes steady and stable to small disturbances. In coaxial jets separated by a thick wall, Michalke [9] and Talamelli and Gavarini [10] shown that an additional wake mode can exist and only this mode become absolute unstable when the wake velocity reaches very low values.

However, in a recent experimental study of Tian et al [1], two self-excited frequencies were found in the frequency spectra. Nevertheless, previous theoretical and numerical studies of the same problem revealed an absolutely unstable region just downstream of the splitter plate containing only a single pinching point associated with the asymmetric mode. The symmetric mode is always found absolutely stable. In order to further investigate this problem, a local and inviscid linear stability analysis is performed. This is done using both shooting method and matrix forming approaches for cross validation. Two separate base flows are constructed to fit the experimental data, extracted from the original experimental study using an image processing code. The first base flow profile is based on a linear interpolation of this data, smoothed out using a diffusion equation, whereas the second base flow profile is based on matched similarity solutions of the boundary layer equations. All nine cases reported in the experimental study, with three different velocity rations and three different Reynolds numbers, were reproduced. Their analysis reveals two pinching points, one for the symmetric mode and another for the asymmetric mode, for some cases. In general, there is a good agreement with the experimental frequencies for all nine cases. It appears that the ability to capture the additional pinching point strongly depends on the momentum thickness of both layers being different. In all previous theoretical and numerical studies, however, these thicknesses were assumed equal.

2 Instability analysis

Linear stability theory (LST) relies on the decomposition of any flow quantity into a steady base flow part and an unsteady part

$$\mathbf{q}(\mathbf{x},t) = \overline{\mathbf{q}}(\mathbf{x}) + \varepsilon\tilde{\mathbf{q}}(\mathbf{x},t), \tag{1}$$

where $\mathbf{x}$ is the space coordinate vector, t is time and $\varepsilon \ll 1$ is a small amplitude. Substituting this equation into the Navier-Stokes equations, subtracting the steady flow and dropping the terms in ε^2 yields the linearised perturbation equations, referred to as the linearised Navier-Stokes equations (LNSE). Once a base flow has been provided, the LNSE may be solved as an initial-boundary-value problem and are valid for any small amplitude perturbation. In the present analysis, the base flow is considered homogeneous along two spatial directions and the local flow assumption is made. The perturbation becomes

$$\tilde{\mathbf{q}} = \hat{\mathbf{q}}(y)e^{i(\alpha x-\omega t)}, \tag{2}$$

where $\hat{\mathbf{q}} = (\hat{u},\hat{v},\hat{p})$, ω is taken to be a real frequency parameter, while the complex eigenvalue α and the associated eigenvector are sought.

The local flow assumption neglects the base flow velocity component transverse to the perturbation motion and considers two base flow spatial directions as homogeneous, such that $\frac{\partial\overline{\mathbf{u}}}{\partial x} = \frac{\partial\overline{\mathbf{u}}}{\partial z} =$

0. This approximation is valid in the present work since $\frac{\partial \bar{\mathbf{u}}}{\partial y} >> \frac{\partial \bar{\mathbf{u}}}{\partial x}$ and only two-dimensional analysis is performed. Table 1 shows the magnitude of the maximum absolute value for three different Reynolds number analysed. As can be seen, in the worse case (Re = 6196) the difference is up to 0.43%. Eigenmode expansions in the directions x is introduced, such that $\frac{\partial \tilde{\mathbf{u}}}{\partial x} = i\alpha\tilde{\mathbf{u}}$. The linearised Navier-Stokes equations in this limit take the form os the system of ordinary differential equations

Table 1 Difference in the magnitude of the maximum absolute value of the base flow derivatives y and x.

Re	Max($\lvert\partial\bar{\mathbf{u}}/\partial y\rvert$)	Max($\lvert\partial\bar{\mathbf{u}}/\partial x\rvert$)
6196	6.737	0.029
15676	12.255	0.025
21020	14.717	0.036

$$\begin{aligned} i\alpha\hat{u} + \hat{v}_y &= 0 \\ L_{1d}\hat{u} - \bar{u}_y\hat{v} - i\alpha\hat{p} + i\omega\hat{u} &= 0 \\ L_{1d}\hat{v} - \hat{p}_y + i\omega\hat{v} &= 0 \end{aligned} \tag{3}$$

where the subscripts x, y denote $\partial/\partial x, \partial/\partial y$, respectively and L_{1d} takes the form of

$$L_{1d} = (1/Re)[(\partial^2/\partial y^2) - \alpha^2] - i\alpha\bar{u} \tag{4}$$

System 3 can be rearranged and written in the form of a single ordinary differential equation of fourth order for the pressure disturbance, known as the Orr-Sommerfeld equation. In the limit $Re \to \infty$, the viscous terms of the Orr-Sommerfeld equation can be dropped, giving rise to the Rayleigh equation

$$\hat{p}'' + \frac{2\,\alpha\,\hat{p}'\bar{u}'}{\omega - \alpha\bar{u}} - \alpha^2\hat{p} = 0. \tag{5}$$

In the present work, both the system 3 as the equation 5 are solved.

3 Base Flow

One of the most important tasks in a linear stability analysis is the correct choice of base flow. As explained by [11], a steady-state solution of the Navier-Stokes equation is the best choice for a base flow, since anything else can introduce forcing terms in the governing equations that might alter the analysis . However, detailed experimental data about the boundary layer flow near the end of the splitter is not provided for the problem being investigated here. Without this information, it becomes difficult to numerically generate a steady-state. Hence, alternative base flows are necessary. First, an image processing code was created to extract the mean base flow from the experimental PIV images. Second, two approaches were employed to fit the data obtained: An uniform valid asymptotic solution (UVAs) and a smoothed interpolation of the experimental data.

3.1 Experimental Data

The experiment were performed in the NOAH water tunnel located at the Graduate Aerospace Laboratories of the California Institute of Technology [1]. The experimental set up consisted of an upstream splitter plate with a thickness of $t = 0.057\,m$ and a length of $L = 3.5\,m$. Particle Image Velocimetry (PIV) was used to measure the unsteady two-dimensional flow field, from which power spectra was generated. All nine flow configurations reported in their experiment [1] are analysed here. Table 2 shows the configurations. The Reynolds number reported was calculated based on water properties at room temperature and pressure, the average velocity of the two streams and the splitter plate thickness. In order to extract base flow profiles from the PIV data and perform a linear stability analysis, an in-house image processing code was built. It follows a series of steps to extract this data. More details are available in [20]. After completing the steps above, the experimental data for a given position in x is achieved. Figure 1 shows an example of three different locations where the base flow is extracted. It is important to notice that it is easier for the code to read smoother transitions in the colors rather than big ones. For in-

Table 2 Experimental flow configurations analysed here [1].

Re	VR	Re	VR	Re	VR
6196	0.93	15185	0.98	21430	1.00
6031	0.46	15676	0.57	22120	0.55
6043	0.30	14810	0.32	21020	0.32

stance, in the x position near the plate, the momentum thickness has a small value, meaning a quick transition between the stream flow and the wake. As a result, the code could not match these points. However, as the x position moves away from the plate, the momentum thickness increases its value, tending to a smoother transition. Therefore, the number of points that the code can match with the scale rises.

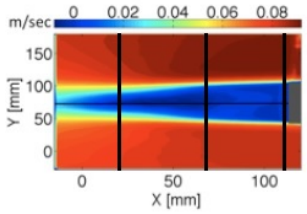

Fig. 1 Example of three different profiles extracted from the PIV flow field experiment performed by [1] with the in-house code.

3.2 Uniform Valid Asymptotic Solution (UVAs)

The next step is to fit those data. As discussed, the first approach is to use Navier-Stokes equations. A similar conservation equation for the incompressible laminar boundary layer problem is given by:

$$2f''' + ff'' = 0 \tag{6}$$

with the boundary conditions: $f(0) = 0$ $f'(-\infty) = 1$ and $f'(\infty) = VR$. VR is the velocity ratio between layers. In order to simulate this equation, a shooting method was chosen. It turns a boundary value problem into an initial value problem to best control the error. The resulting system is integrated towards the already known boundary condition. In order to fit the experimental data, the profile was breakdown in two profiles in the $x = 0$ position. The left side and the right side are calculated separately with equations 6 and the initial conditions to fit the experimental data. After that the method of matched asymptotic expansions is used to combine the solutions. In a few words, this method tells us to add both solutions and subtract the common terms. The reader is referred to the books by Dyke[12] and Kevorkian and Cole [13] for more details. Although such solutions are not unique, they are as accurate as the asymptotic solutions used to form them. Figure 2 shows the experimental data (triangles) with the UVAs (continuous line) for the three different x positions showed previously. As

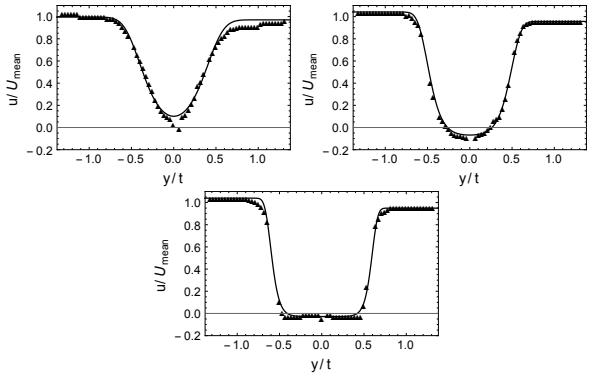

Fig. 2 Profiles extracted in the three different x positions. The experimental data are showed in triangles and the UVAs are showed in continuous line.

can be seen, very good agreement is achieved in two of the tree cases. When the base flow moves away from the plate, the wake region decreases until it disappears. As a result, their derivative in the transition of the two streams tends to an abrupt change, different from the behaviour in the wake region. Therefore, the UVAs method has difficulty to capture this change. However, it is important to interpret the physics in the results.

3.3 Interpolation

The second method used to fit the data was a direct interpolation through the experimental data obtained from the code. A first order interpolation was chosen. This approach has two important problems to consider. The fist one is due to the fact that it doesn't obey the Navier-Stokes equation, introducing forcing terms in the equation. Teixeira and Alves [11] explained the importance of an accurate base flow in a linear stability analysis. The second one is due to the high frequencies that are present in the images from the experimental data. Although nothing can be done in the first one, the second problem can be improved. Therefore, a diffusion equation is used

in order to smooth the high frequencies present in the experimental data. Equations 7 and 8 show a diffusion equation which the appropriated initial and boundary condition. *IP* represents the experimental data interpolation and *yL* and *yR* represent the left and right position which bounds the data. The diffusivity α is chosen to be a function of y, because more diffusivity is needed where higher oscillations are present and less where almost or none oscillations are present.

$$\frac{\partial u}{\partial t} = \alpha(y)\,\frac{\partial^2 u}{\partial y^2} \tag{7}$$

$$\begin{aligned} u(0,y) &= IP(y) \\ u(t,yL) &= IP(yL) \\ u(t,yR) &= IP(yR) \end{aligned} \tag{8}$$

Figure 3 shows the resulting profile after applying diffusivity. In these three examples, the regions which higher oscillations were in the wake. Hence, more diffusivity was employed. The dashed lines represent the diffusivity function, normalized in order to fit in the graphics range. As a result from this methodology, it can be seen

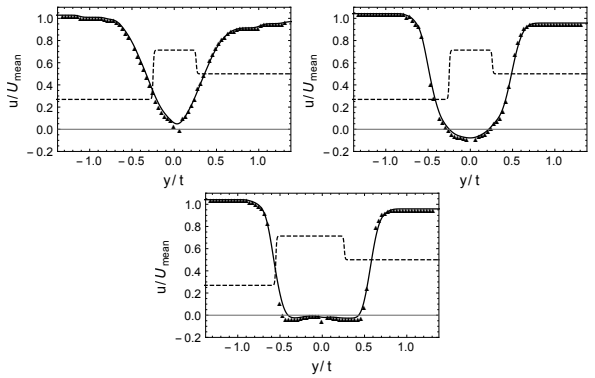

Fig. 3 Profiles extracted in the three different x positions. The experimental data is showed in triangles, the interpolation is showed in continuous line and the diffusivity α is showed in dashed lines.

that qualitatively the profiles look like the profiles obtained from the UVAs method. Two from the three cases have very good agreement while the same profile in the two methodologies have the same problem when a beak is present in the profile.

4 Numerical Methods

4.1 Matrix Forming

When using the matrix forming method, system (3) is discretized using second, fourth, sixth and eighth order finite differences on a non-uniform grid, leading to a non-linear spatial eigenvalue problem in the form of

$$\mathbf{A}.\hat{\mathbf{q}} = \sum_{k=1}^{2} \alpha^k \mathbf{B_k}.\hat{\mathbf{q}} \tag{9}$$

where $\mathbf{A}$ and $\mathbf{B}$ are block matrices. However, using the companion method [14], an auxiliary vector $\hat{\mathbf{q}}^* = [\hat{u}, \hat{v}, \hat{p}, \alpha\hat{u}, \alpha\hat{v}]$ is define and it is possible to write a linear version of the same problem in the form of

$$\mathbf{A}.\hat{\mathbf{q}}^* = \alpha\,\mathbf{B}.\hat{\mathbf{q}}^* \tag{10}$$

Once again, in this analysis, $\omega \in \Re$ is a real frequency parameter, while $\alpha \in \mathbb{C}$ is the sought eigenvalue, the real part of which is related with the periodicity length along the homogeneous spatial direction x, through $\alpha_r = 2\pi/L_x$ and the imaginary part α_i is the spatial amplification/damping rate.

In order to solve the eigenvalue problem, the Arnoldi algorithm [15] is employed, combined with the Lapack library [17] to solve the LU-Decomposition and back substituting. The Arnoldi algorithm delivers a chosen number of eigenvalues around a specific estimate value. Such value is set around the most unstable eigenvalue. The computational cost employing the Arnoldi algorithm is notoriously reduced in comparison with the classical QZ method. More detail can be found in literature [16, 15].

4.2 Shooting Method

The other method programmed was a shooting method to solve the Rayleigh equation 5. Since the goal are spatially growing solutions, the procedure used to solve the pressure disturbance equation was the same as [18]. The first step is to obtain asymptotic solutions for the pressure in the limits of $y \to -\infty$ and $y \to \infty$, since it is known that the base flow derivative is zero in both these limits.

$$-\alpha^2 \hat{p}[y] + \hat{p}''[y] = 0 \tag{11}$$

Since the pressure disturbance must vanish both when $y \to -\infty$ and $y \to \infty$, equation 11 yields in these limits,

$$\hat{p}[y] = C_1 e^{y\alpha} \qquad \hat{p}[y] = C_2 e^{-y\alpha} \tag{12}$$

It is important to notice that, in order to avoid singularities at both limits, the numerical integration must be started at finite non-zero values of y, where the base flow derivative is $\approx O^{-12}$. If the order of accuracy is increased further, the size of the domain increases and, although the accuracy of the solution improves, it becomes very hard to track the regular eigenmodes. Since an eigenvalue problem is solved, the solution for the pressure disturbance in both limits can be normalised, avoiding the need to find the constants C_1 and C_2,

$$p_L[y] = \frac{\hat{p}[y]}{C_1} \qquad p_R[y] = \frac{\hat{p}[y]}{C_2} \tag{13}$$

This way, equation 5 is numerically integrated from both sides of the far field (namely p_L and p_R) towards the centre of the domain, where the pressure disturbance and its derivative should be continuous. The numerical procedure will iterate α, on the complex plane, until the matching conditions are satisfied for a given value of ω. Therefore, a newton-type root finding can solve the Wronskian

$$p_L[0]\ p'_R[0] - p_R[0]\ p'_L[0] = 0. \tag{14}$$

If this hypothesis is not satisfied, a new value is assigned to the wave-number in a process that is repeated until the Wronskian is equal zero. The problem then comes down to finding an initial estimate for the wave-number that approximately satisfies the so-called dispersion relation $f(\alpha,\omega) = 0$. In order to do so, there are two possibilities. The first one is to created a mesh for the real and imaginary parts of α. A contour plot of the interpolated zero real and imaginary parts of the dispersion relation is made, for a fixed frequency. The point of intersection between these two curves is the graphical estimate for the complex wave-number. As the frequency is increased, extrapolation is employed to generate new estimates for the next wave-number. The second option is to use matrix-forming results to estimate the initial guess of the complex wave-number. Then, the same extrapolation is use to estimate the next eigenvalues.

4.3 Novel Methodology

Obtaining the onset of absolute instability from a differential dispersion relation may be difficult. The to-date methods to locate the so-called saddle points can either require expensive computational coast or only track saddle points connected by continuity [19]. In the novel methodology provided by Alves and Hirata [19] the zero group velocity condition is applied directly to the differential dispersion relation. As a result, it is possible to search for arbitrary saddle points and also verify their causality. Taking the derivative of equation 5 with respects to α leads to a new dispersion relation

$$\hat{p}''_\alpha + \frac{2\bar{u}\alpha\hat{p}'_\alpha}{(\omega - \alpha\bar{u})} - \alpha^2\hat{p}_\alpha = 2\alpha\hat{p} - \frac{2\omega\hat{p}'\bar{u}}{(\omega - \alpha\bar{u})^2} \tag{15}$$

where $\hat{p}_\alpha = d\hat{p}/d\alpha$. Equation 15 is solved with the same shooting method procedure showed to solve equation 5, where the constants disappear if it is solved to the normalized solution.

5 Results

5.1 Instability Analysis

Each nine cases proposed will be analysed separately, in three major cases with the same velocity ratio and varying the Reynolds number. Table 2 shows the cases. The case with velocity ratio VR $\approx$ 1 is called case 1, the case with VR $\approx$ 0.5 is the case 2 and the case with VR $\approx$ 0.3 is the case 3. The case with lower Reynolds number is referred as case 1-1, 2-1, 3-1, the case with medium Reynolds number as case 1-2, 2-2, 3-2 and the case with high Reynolds number is referred as case 1-3, 2-3, 3-3. Since the lowest Reynolds number is still high enough to run a inviscid instability the only influence of the Reynolds number in the following cases is in the momentum thickness. In other words, the larger is the Reynolds number, the smaller the momentum thickness. To make the parameters non-dimensional, the plate thickness (t = 57 mm) and the average velocity between the two streams (U_{mean} = [U1 + U2]/2)

were used, as in accordance to the experiment [1]. All units presented in x are in millimetres. The scale in the direction x also follows the experimental paper, where the plate is located in $x = 110$ and the flow develops in direction to $x = 0$. In all cases (1,2,3) the range of the graphic is kept the same to facilitate comparison between different Reynolds number.

The shooting method was implemented in the software MATHEMATICA and the matrix forming in FORTRAN 90.

5.1.1 Case 1

The first group of case analysed is when the velocity ratio between the two streams is kept approximately the same (VR $\approx$ 1). The three different Reynolds number are varied.

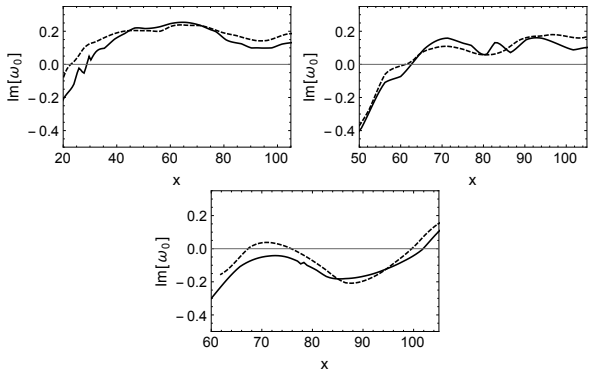

Fig. 4 Case 1: Imaginary part of ω_0. The solid line is referred to the UVA's base flow and the dashed line to the direct interpolation of the data.

Figure 4 present the imaginary part of ω_0. The solid lines represent the UVA's base flow and the dashed line the direct interpolation through the experimental data. As it can be seen, the flow leaves the plate already in an absolute regime in both methods, since the imaginary part of the frequency is positive. This is an expected behaviour in a scenario where the stream velocities are kept approximately the same.

5.1.2 Case 2

The second group of case analysed is when the velocity ratio between the two streams is approximately 0.5 (VR $\approx$ 0.5). Figure 5 presents the imaginary part of ω_0. Following the same

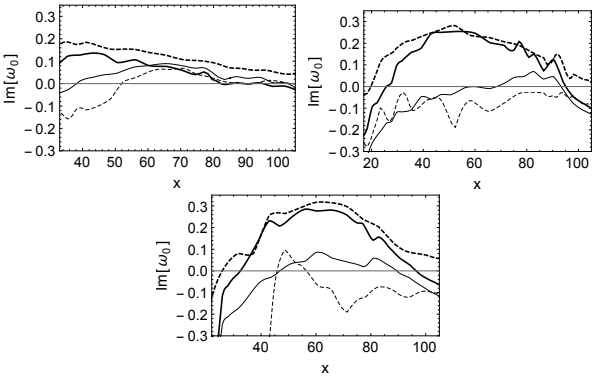

Fig. 5 Case 2: Imaginary part of ω_0. The solid line is referred to the UVA's base flow and the dashed line to the direct interpolation of the data. The bold is related to mode 1 and the thin to the mode 2.

label, the solid lines represent the UVA's base flow and the dashed line the direct interpolation through the experimental data. However, now the two modes were captured in the shooting method. The bold is related to the first mode (anti-symmetric) and the thin to the second mode (symmetric). As it can be seen, since the velocity ratio is not the same, the flows not necessarily leaves the plate in an absolute regime. Moreover, and the most important result, the two modes becomes absolute unstable in different positions along x direction. Both the UVA's base flow as the interpolated present the same behaviour. It is also important to notice that the temporal growth rate is highly sensible to the base flow, and that can be the reason of the variations in the imaginary parts.

5.1.3 Case 3

The third and last group of cases analysed is when the velocity ratio between the two streams is approximately 0.3 (VR $\approx$ 0.3).

Figure 6 presents the real and imaginary part of ω_0. Unlike the previous cases, this time, the second mode from the interpolated base flow has smaller temporal growth rate as in comparison with the UVA's base flow. As a result, the UVA's base flow has two pinching points and, like the case 2, they occur separately.

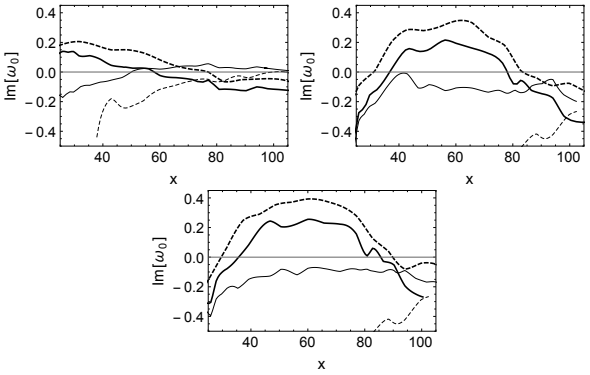

Fig. 6 Case 3: Imaginary part of ω_0. The solid line is referred to the UVA's base flow and the dashed line to the direct interpolation of the data. The bold is related to mode 1 and the thin to the mode 2.

5.2 Collision Check

In order to prove that the saddle point in the onset of absolute instability presented in 4 - 6 is indeed a pinching point, a collision check was performed. In this check, in order to have a pinching point, the mode that comes from the bottom of the complex wave-number (branch α^+) has to pinch with the mode coming from above (branch α^-). For this analysis, only the UVA's base flow was checked. To do this, the matrix forming method with the Arnoldi iteration was used. Figure 7 shows the complex wave-number plane with $\mathrm{Im}[\omega] = 0$. Three position were analysed: before ($x = 26$), in the pinching ($x = 27$) and after ($x = 28$). The anti-symmetrical mode is the mode that pinches with the branch α^- and represents the transition of convective to absolute instability. In this case, the symmetrical mode remains with a low spatial growth rate.

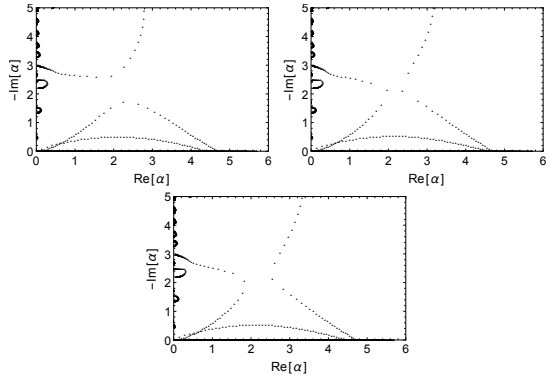

Fig. 7 Matrix forming method with $Im[\omega] = 0$ for the case 1-1. The positions $x = 26$ (upper left), $x = 27$ (upper right) and $x = 28$ (bottom) show the pinching point.

5.3 Comparison with Experiments

In order to compare the numerical results with the experimental, a band of the onset of absolute instability was plotted together with the experimental spectra. Figure 8 presents the results.

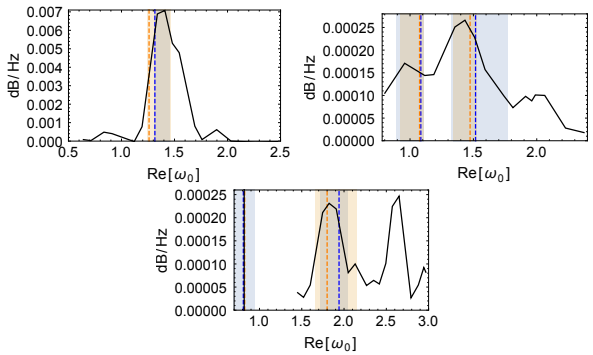

Fig. 8 Experimental frequency spectra (solid line), frequency region of numerical absolute instability (blue band → UVAs, orange band → Interpolation) with the maximum frequency in the absolute regime (dashed line). Upper left: Case 1-1, Upper right: Case 2-1 and Bottom: Case 3-1.

The experimental frequency spectra from [1] correspond to the solid black line. Together with this frequency, a band containing the region where the flow is absolute unstable (i.e. $\mathrm{Im}[\omega_0] > 0$) is plotted. This can be done by looking at the figures 4 - 6 and select the related frequencies. Together with this band, the maximum value of the frequency found in the absolute region is selected and plotted as a dashed line. In figure 8 the blue band and dashed line correspond to the UVAs method whereas the orange band and dashed line correspond to the interpolation. Unfortunately, in the case 3-1 at the bottom of figure, the experimental spectra doesn't show what happens in the range of frequencies lower than 1.5. However, the instability analysis using the UVAs base flow shows that both modes can be absolute unstable and a second blue band is marked. Having this results, the high frequency that appears can be understood as a harmonic of the two other modes.

In fact, if we subtract the higher experimental frequency (≈ 2.7) from the other experimental frequency (≈ 1.9) we get ≈ 0.9, represented as a solid black line. As it can be seen, it matches inside the absolute region of the second mode, with the peak almost coinciding.

In the last analysis of this case, a contour plot of the cross-stream velocity v from the experiment is plotted together with the imaginary frequency calculated (Fig. 9). A perfect antisymmetry is observed in the case 1-1, which was expected, since the velocity ratio is approximately 1. Moreover, the region of recirculation matches with the region where absolute instability was found. In the case 2-1 as well as in the case 3-1, the antisymmetry is lost, specially in the wake region.

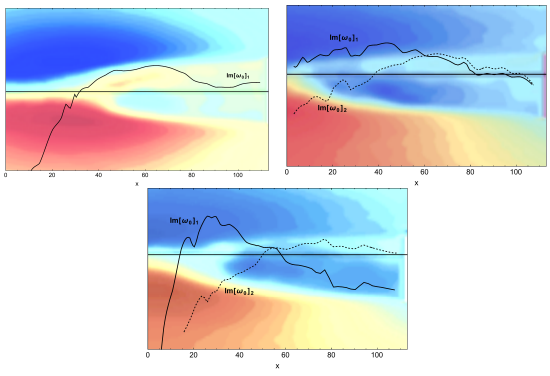

Fig. 9 Cross-stream velocity v provided by together with the imaginary part of the frequency numerically calculated for Case 1-1: upper right, Case 2-1: upper left and Case 3-1: bottom.

6 Summary and Conclusion

The aim of this investigation was to re-evaluated the stability analysis in a mixing layer/wake interaction where experimental results indicated the presence of two distinct fundamental frequencies. It was presented that the origin and reason for this phenomenon is due to multiple self-excitation frequency found in the near field. To the authors best knowledge, such results were never presented for significant physical flows in the literature.

The first step to perform a linear stability analysis was the study of a accurate base flow. Since experimental results were provided as a mean flow and in PIV data, a code was build to capture profiles along x direction. After that, two approaches were followed: a similar solution of the Navier-Stokes equations and a direct interpolation though these data. The second step was the solution of the stability equations itself. Two methods were used: Matrix Forming and Shooting method. The shooting method was used to solve the Rayleigh equation and the Matrix Forming to solve the 1D linearised Navier-Stokes equation.

Nine different cases were analysed, where different velocity ratio and Reynolds number were imposed. In all cases, the saddle points found were proved to be indeed a pinching point. When comparing the two base flow used, a qualitative behaviour could be noticed in the complex frequency. For each velocity ratio, the temporal growth rate was plotted together with the experimental mean cross-stream velocity v. The antisymmetry seeing in the cases 1 (VR ≈ 1) was apparently demolish for the other cases. It was also noticed that in the cases 1-1 the region of absolute instability coincided with the wake region.

As a major goal of the presenter work, the experimental fundamental frequencies were plotted against the band of absolute region of the modes. The numerical frequency with the most amplified temporal growth rate were also plotted. It was concluded that the presence of more than one peak in the spectra can be related to two reasons: a higher harmonic as a combination from other frequencies and the existence of a transition from convective to absolute unstable in the symmetrical mode (also called mode 2), provoking a new band of absolute frequencies. Thereby, the present of all frequency peaks in the experimental spectra could be explained.

References

[1] Tian V, McKeon B and Leyva I. Split Stream flow past a blunt trailing edge with application combustion instabilities. *48th AIAA/ASME/SAE/ASEE Joint Propulsion Conference & Exhibit*, pp 3807, 2012

[2] Boldman D R, P F Brinich and M E Goldstein. Vortex shedding from a blunt trailing edge

with equal and unequal external mean velocities. *Journal of Fluid Mechanics* Vol. 75, No. 4, pp 721-735, 1976.

[3] Koch W. Local instability characteristics and frequency determination of self-excited wake flows. *Journal of Sound and Vibration* Vol. 99, No. 1, pp 53-83, 1985.

[4] Wallace D and Redekopp LG. Linear instability characteristics of wake-shear layers. *Physics of Fluids A: Fluid Dynamics*, Vol. 4, No. 1, pp 189-191, 1992.

[5] Hammond DA and Redekopp LG. Global dynamics of symmetric and asymmetric wakes. *Journal of Fluid Mechanics*, Vol. 331, pp 231-260, 1997.

[6] Chomaz JM. Transition to turbulence in open flows: what linear and fully nonlinear local and global theories tell us. *European Journal of Mechanics- B/Fluids*, Vol. 23, No. 3, pp 385-399, 2004.

[7] Laizet S, Lardeau S and Lamballais E. Direct numerical simulation of a mixing layer downstream a thick splitter plate. *Physics of Fluids*, Vol. 22, No. 1, pp 015104, 2010.

[8] Biancofiore L, Gallaire F and Pasquetti R. Influence of confinement on a two-dimensional wake. *Journal of Fluid Mechanics*, Vol. 688, pp 297-320, 2011.

[9] Michalke A. On the influence of a wake on the inviscid instability of a circular jet with external flow. *European journal of mechanics. B, Fluids*, Vol. 12, No. 5, pp 579-595, 1993.

[10] Talamelli A and Gavarini I. Linear instability characteristics of incompressible coaxial jets. *Flow, turbulence and combustion*, Vol. 76, No. 3, pp 221-240, 2006.

[11] Teixeira R and Alves L. Minimal gain marching schemes: searching for unstable steady-states with unsteady solvers. *Theoretical and Computational Fluid Dynamics*, pp 1-15, 2017

[12] Dyke M Van. Perturbation methods in fluid mechanics *Applied mathematics and mechanics*, Vol. 8, New York [etc.]: Academic Press, 1964.

[13] Kevorkian J. and Cole J D. Perturbation methods in applied mathematics, *Springer Science & Business Media*, Vol. 34, 2013

[14] Bridges TJ and Morris PJ. Differential eigenvalue problems in which the parameter appears nonlinearly. *Journal of Computational Physics*, Vol. 55, No. 3, pp 437-460, 1984

[15] Saad, Y. Variations on Arnoldi's method for computing eigenelements of large unsymmetric matrices. *Linear algebra and its applications*, Vol. 34, pp.269-295, 1980.

[16] Theofilis V. Advances in global linear instability analysis of nonparallel and three-dimensional flows *Progress in aerospace sciences*, Vol. 39, No. 4, pp 249-315, 2003.

[17] Anderson, Edward and Bai, Zhaojun and Bischof, Christian and Blackford, L Susan and Demmel, James and Dongarra, Jack and Du Croz, Jeremy and Greenbaum, Anne and Hammarling, Sven and McKenney, Alan and others. LAPACK Users' guide, SIAM, 1999.

[18] Michalke, Alfons. On spatially growing disturbances in an inviscid shear layer. *Journal of Fluid Mechanics*, Vol. 23, No. 03, pp. 521-544, 1965.

[19] Alves L and Hirata S. Locating Saddle Points in Differential Dispersion Relations. *Proceedings of the XXIV ICTAM*, 2016.

[20] Quintanilha Junior, HRDA and Alves L. On the Existence of Multiple Self-Excitation Frequencies in the Instability of Interacting Planar Mixing Layer and Wake. *Masters thesis*, UFF, 2017.

7 Contact Author Email Address

leonardo.alves@gmail.com

Copyright Statement